Walking robot movement on non-smooth surface controlled by pressure sensor

T. K. Maiti*, Y. Ochi, D. Navarro, M. Miura-Mattausch and H. J. Mattausch

HiSIM Research Center, Hiroshima University, Higashi-Hiroshima, 739-8530, Japan

*Corresponding author

DOI: 10.5185/amlett.2018.1878
www.vbripress.com/aml

Abstract

In this letter, we focus on the robot movement on non-smooth ground-surface, detected by pressure sensor. A simulation tool has been developed to study the robot motion according to the ground-surface condition change. The effect of the robot-foot contact with the ground-surface is considered by elastic properties to the ground. We performed simulation analyses for various surface conditions to control the robot dynamics with respect to pressure sensing data that incorporates the two-way interactions between robot and ground. We upgraded the robot by implementing the pressure sensors under its foot, to measure the real-time contact force between foot and ground-surface. The obtained sensing data is used to analyse the surface condition, for controlling robot-leg movement horizontally along the ground-surface. Consequently, the analysis results guide us to improve the motion of a real self-controlled walking robot. Copyright © 2018 VBRI Press.

Keywords: Pressure sensor, electro-mechanical, walking robot, motion control, system simulation.

Introduction

Over the last two decades and more, a variety of pressure sensors have been reported for robots, such as piezoresistive, capacitive, piezoelectric, optical pressure sensors and so on [**1-12**]. Among those sensors, a piezoresistive pressure sensor is more capable to measure the interaction force between robot and ground-surface with a higher degree of temporal and spatial resolution than others [**12, 13**] which allows to learn the structural properties of an object such as size, shape, texture, etc. for manipulation [**12-14**]. It also helps the robot to understand the interaction between robot-foot and real ground-surface, which depends on their weight distribution, hardness properties of ground, and touch conditions of ground surface. Therefore, pressure-sensing-based ground-condition detection is an important investigation for robot movement [**15-17**]. Especially, when the robot moves on non-smooth [see **Fig. 1(a)**] ground-surfaces, it observes dynamically varying pressure on the two individual legs, which must be considered for the robot's smooth movement [**15**]. Previous reports have covered the robot mechanical-dynamics, which are only based on predefined control conditions and are not self-controlled with foot pressure. Even though the foot pressure depends on ground-surface conditions, the reports do not consider the detail descriptions of foot-contact forces, static and dramatic responses, as well as the time-domain pressure-control-signal conditions [see **Fig. 1(b)**]. Additionally, the detail description of electrical schematic of the robot controller is still missing, which is necessary for real pressure-sensor-based self-controlled walking-robot development [**18-20**].

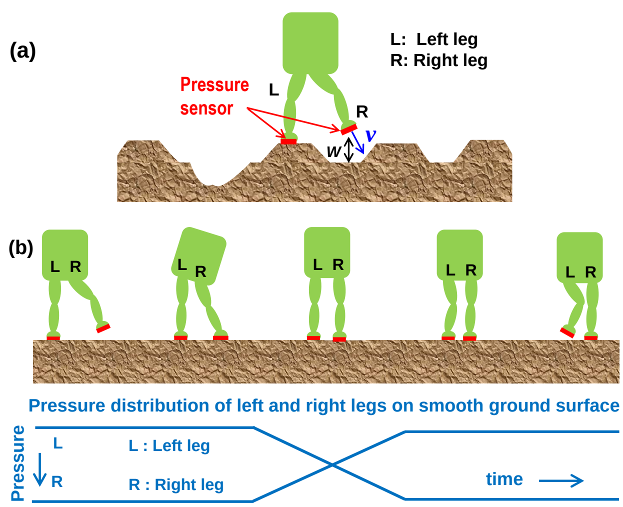

Fig. 1. (a) Robot consists of two legs that can sense the dynamic pressure change via piezoresistive pressure sensor, induced by ground-surface condition, (b) Illustrates a schematic picture of transient pressure responses of two legs on a smooth ground-surface.

In this work, we focus on the robot foot-contact pressure detection with piezoresistive pressure sensor for robot movement on unknown ground surfaces, which does not required predefined information about the ground condition. We performed the robot system simulation with the development of a pressure sensor model, to study the pressure changes, detected by the sensors, according to the ground-surface-condition change. The simulation considered the two-way ground interactions with the robot (robot ↔ ground). Finally, we utilized the simulation analysis to study the pressure-sensor-driven biped motion of a real robot KHR-3HV manufactured by Kondo Kagaku Co. Ltd [**21**].

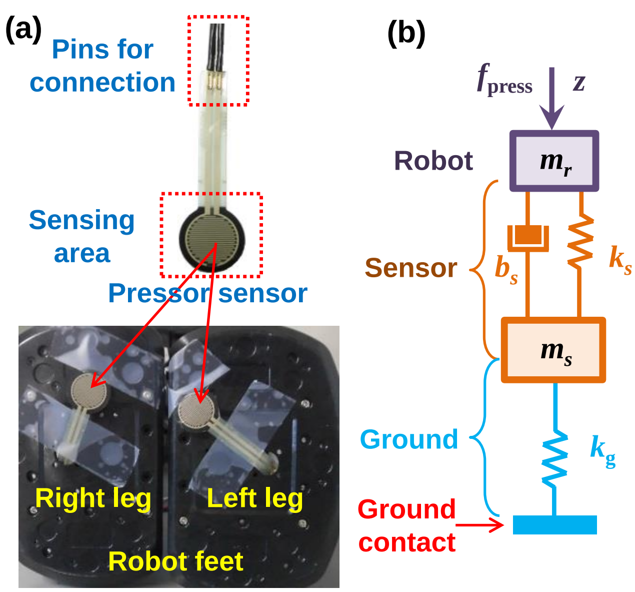

Fig. 2. (a) Pressure sensor which is embedded in robot foot to sense the force/pressure between robot legs and ground-surface, (b) An equivalent mechanical component of the developed robot-system [see **Fig. 1(a)**], where *m* and *k* are the robot mass and elastic constant, respectively. Suffixes *r*, *s*, and *g* represent the robot body, pressure sensor, and ground respectively.

Pressure Sensor

Two *flexiforce* pressure sensors are embedded in the robot foot [see **Fig. 2(a)**] for contact pressure detection, manufactured by Tekscan, Inc. [**22**]. The sensor material is piezoresistive in nature, sandwiched in-between two flexible polyester layers with printed silver conductors on the inner side of each layer. Two pins are provided, which are used for the connection with micro-controller via AD (analog-to-digital) converter [**21**].

Prior to the implementation of the pressure-sensor-driven robot-control algorithm in a micro-controller, we developed a pressure sensor model for robot-movement simulation. The model is developed with the consideration of both electrical and mechanical signals analysis which relates the sensor structure deformation due to the robot foot pressure (mechanical domain) to a transduced voltage (electrical domain) [**23, 24**]. We assume that the sensor is subjected to the foot force f_{press}, along *z*-direction (vertical to ground) which is counter-balanced by sensor spring force f_s, damping force f_d, and mass force f_m [see **Fig. 2(b)**]. The developed formulations of the force components and the total force are summarized in **Table I**.

Table I. Formulations of force components.

Name	Formulation
Spring force	$f_s = k_s \times z$
Damping force	$f_d = b_s \times \dot{z}$
Mass force	$f_m = m_s \times \dot{v}$
Total force	$f_{press} = f_m + f_d + f_s$

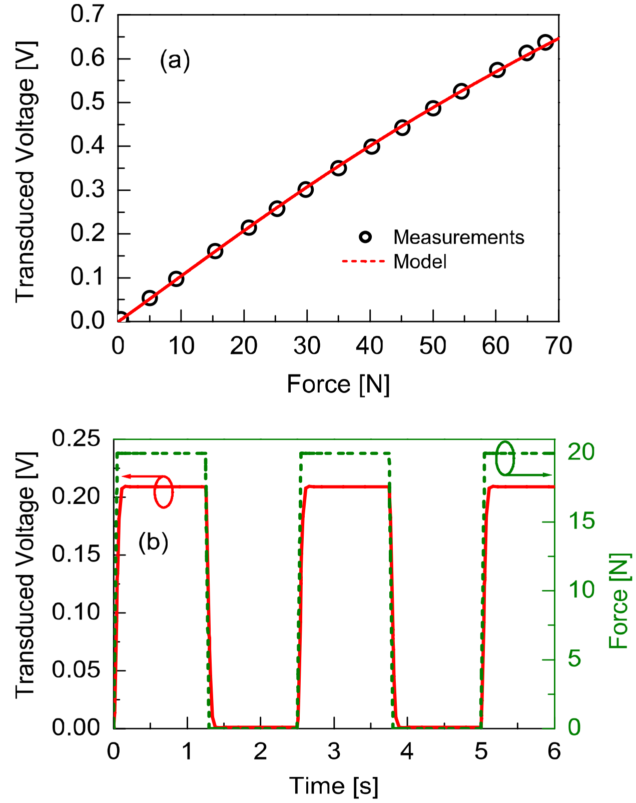

Fig. 3. (a) Pressure variation *vs.* force comparison between developed model (solid line) and measurements (symbols), (b) Modeled transient response of transduced voltage signal (solid line) for periodic 20N mechanical force (dotted line).

Here, velocity $v = \dot{z} = dz/dt$ and acceleration $\dot{v} = d\dot{z}/dt$ are both along the z-axis, and the sensor has stiffness k_s, damping b_s, and seismic mass m_s. If f_{press} deforms the sensor structure with an amount *z*, then according to Newton's second law

$$\begin{cases} \dot{v} = \dfrac{1}{m_s}\left(-b_s v - k_s z - k_n z^3 + f_{press}\right) \\ v = \dot{z} = \dfrac{dz}{dt} \end{cases} \quad (1)$$

Here, the spring force coefficient k_n [N/m^3] is added to consider the non-linear effect of pressure-sensor responses [**25**]. Differential equation (1) solves *z* which is used to determine the mechanical stress σ, generated inside the sensor material due to the foot-contact force, derived as

$$\sigma = \frac{96}{5} \cdot \frac{HWY}{L^4}\left(z^2 - L \cdot z\right) \quad (2)$$

Here, *Y* is Young's modulus of the pressure sensor material, while *L*, *W*, and *H* are length, width, and height of the sensor, respectively. The sensor transduces the pressure (force per unit area) into a voltage signal [**26, 27**] via generation of mechanical stress σ in the piezo-resistive material. If *R* and R_0 are mechanical stress dependent and independent resistances of the sensor having piezo-resistive co-efficient π, then *R* can be expressed as $R = R_0(1 + \pi\sigma)$ which gives the relation between current *I* and transduced voltage *V* [**28, 29**].

$$V = I \cdot R_0 (1 + \pi\sigma) \quad (3)$$

Equations (1) and (3) are developed and implemented with canonical conjugate relations f_{press} to v and V to I, respectively, under the energy conservation condition, where the mechanical components of the kinetic discipline relate linear velocity to linear force, while the electrical discipline relates V to I. Here mechanical power, $f_{press} \times v$ is transformed to the equivalent electric power, $V \times I$ via interactions between robot foot and ground-surface and vice versa. We compared transduced voltage variation as a function of force with measurements, done using a *flexiforce* pressure sensor [**22**] [see **Fig. 3(a)**]. Simulated transient transduced voltage with external periodic 20N force, obtained using the developed model, is depicted in **Fig. 3(b)**.

Robot-System Simulation

The robot system employs two legs which are connected with pressure sensors, transducing mechanical force to electrical signals [see **Fig. 1(a)**]. The detection characteristics of the ground-surface, with which robot is in contact, is investigated with simulation. We propose contact-event effects such as contact timing (leg contact on ground at different positions and heights), direction of contact force, friction information, flexible properties of ground- surface, by using the concepts of transit-pressure delay, τ_n and elasticity coefficient, k_g [see **Fig. 2(b)**]. The detected force dynamics due to the surface conditions are modeled with τ_n together with k_g as

$$\begin{cases} v(t) = \dfrac{dx(t)}{dt_i} \\ f(t) = m_r \dfrac{dv(t)}{dt_i} + k_g x(t) \end{cases} \quad (4)$$

$$\begin{cases} \tau_n = \dfrac{W}{v} \\ t_i = t_i + \tau_n \end{cases} \quad (5)$$

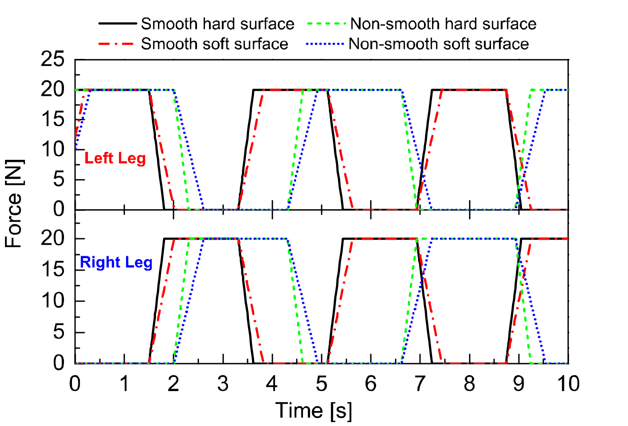

Fig. 4. Effect of contacting events such as soft ground, leg-contact height and depth are considered in terms of pressure delay, τ_n and k_g used for pressure sensing robot control system simulation.

Here m_r, k_g, τ_n, and W are robot body mass, ground hardness coefficient, transit-delay, and depth of the contact surface, respectively. Force responses for smooth-hard, smooth-soft, non-smooth-hard and non-smooth-soft surface conditions are depicted in **Fig. 4**. The information of different τ_n values provides the real pressure-detection condition for the pressure sensor to generate the transduced voltage for control-signal generation to drive the servo-motor that results in robot motion [**30**], especially for robot-leg manipulation. The contact-forces information is used for robot dynamics simulation, performed with our robot-system-simulation tool [**23**] which is based on an equivalent-circuit-network model, developed under the energy-conservation condition in terms of respective potential (examples: V and f_{pres} in electrical and mechanical domains, respectively) and flow (examples: I and v in electrical and mechanical domains, respectively) quantities to incorporate the two-way interactions (robot ↔ ground) in the robot system [**24**]. The time-domain trajectories of robot-leg positions for smooth-hard, smooth-soft, non-smooth-hard and non-smooth-soft ground surfaces are depicted in **Fig. 5(a)**. A zoomed view of **Fig. 5(a)** is illustrated in **Fig. 5(b)**, showing a clear dependence of leg position on contact-event conditions. All figures show the movement of legs along x-direction, demonstrating that the left-leg supports its body while right-leg is in motion and has legs support exchange periodically until 10 seconds. Please note that when the left leg in-touch with the ground surface, it senses the contact force to control the right-leg movement and vice versa. We used this robot system simulation

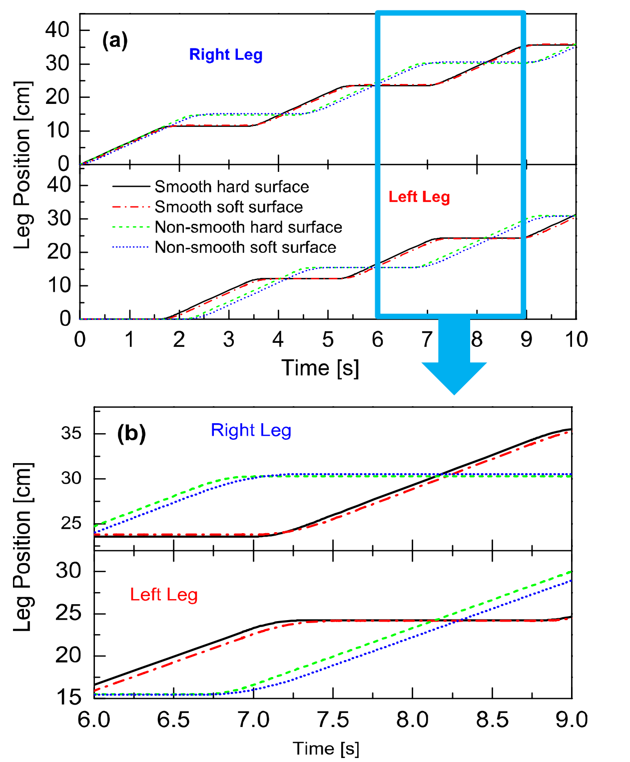

Fig. 5. (a) Simulated left leg and right leg positions of robot, corresponding to transient foot contact force [see **Fig. 4**], are depicted, (b) Shows a zoomed view of **Fig. 5(a)** with clear delay effect on leg positions.

analysis, which guided us to develop our foot-contact pressure-control algorithm for real robot development, which is described in next section. Please note that the time required for robot-leg movement on a smooth-hard surface is smaller than for the other ground- surface conditions, reflecting the transit-delay τ_n.

Robot Development

We performed the experiments to confirm the foot-contact-detection method by developing and implementing a pressure-sensing-data-driven control algorithm in the robot's micro-computer [see **Table II**]. We conducted the experiments for two different foot-contact conditions with the ground-surface i.e., smooth and non-smooth hard-surface-contact conditions to confirm the robustness of our proposed method. We upgraded the hardware of the KHR-3HV robot by embedding pressure sensors in its foot [see **Fig. 2(a)**]. The pressure sensors and the micro-computer of the robot work together for sensing the foot-contact pressure. When the sensor is in contact with the ground it senses the force which decreases the resistance of the sensor to a lower value than for the untouched condition. Utilizing this property of the sensor, we measured the foot-contact force.

Table II. Developed algorithm for foot-contact pressure driven robot-leg movements.

Algorithm: Foot-contact-pressure-driven leg motion
Input: Transduced voltage from pressure sensor
Output: Motion of robot legs
initial: stable position
for (***i*** from **1** to number of foot-steps) **do**
  if (left leg transduced voltage > reference voltage) **then** move right leg
  end if
  if (right leg transduced voltage > reference voltage) **then** move left leg
 end if
end for
return to stable position

The sensing data flow for leg-motion control is depicted in **Fig. 6(a)**. The robot micro-computer senses the transduced left-leg and right-leg sensing voltages V_L and V_R, respectively via AD converter [**21**]. We also defined a reference voltage V_{REF} in the micro-computer memory to compare the contact force for leg-movement control. **Fig. 6(b)** shows the stable condition of the robot when both legs are in touched the ground-surface with $V_L = V_R \leq V_{REF}$, whereas **Figs. 6(c)** and **(d)** depicted the right-leg and left-leg movement when $V_L > V_{REF}$ and $V_R > V_{REF}$, respectively. **Fig. 6(e)** shows the robot leg position on non-smooth ground-surface which reflects the time-domain contact-force transit delay during leg movement. To verify the time-domain sensor-information variation, we developed a pressure-sensor analyzer using an Arduino Uno microcontroller and two pressure sensors [**31**]. We determined the contact force with the measured transuded voltages $V_L(t_i)$ and $V_R(t_i)$ for the robot movement on smooth ground as well as $V_L(t_i + \tau_n)$ and $V_R(t_i + \tau_n)$ for the robot movement on non-smooth ground using the developed analyzer. Here τ_n is the transit delay occurring due to non-smoothness properties of the ground-surface. **Fig. 6(f)** illustrates real time foot-contact pressure responses for different ground-surface conditions. Please note that the transit delay is observed in case of robot movement on non-smooth surface, which agrees with our simulation [see **Fig. 4**].

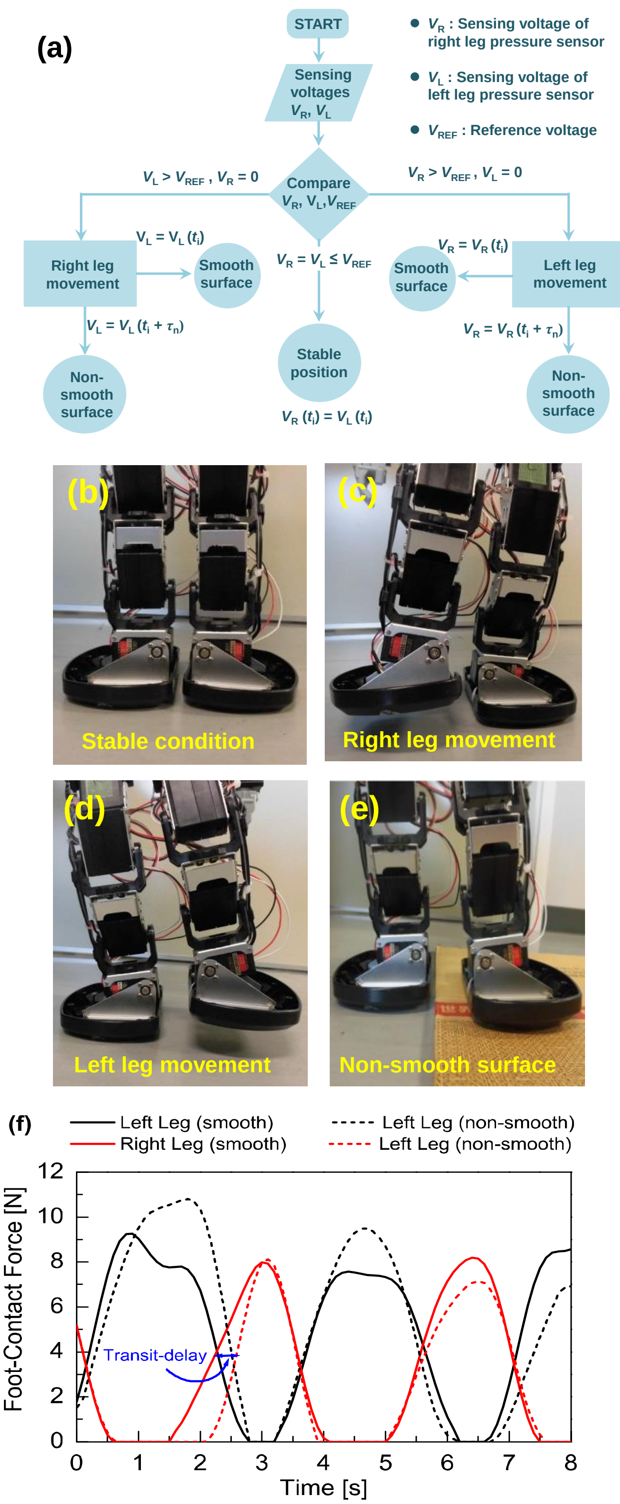

Fig. 6. (a) Sensor data flow to define the foot contact condition for robot-leg-movement control, (b)-(e) Shows real robot movement that is driven by foot-contact forces, and (f) Real-time transient foot-contact-force measurements.

Conclusion

In this work, we presented a method of pressure-sensor-driven foot-contact surface-force detection for electro-mechanical control of walking robot movement. We performed both the simulation and experimental investigations by developing the model for our system-simulation tool and the real hardware, respectively. The simulation analyses guided us to develop a real robot which is upgraded by embedding the pressure sensors under its feet that acquires the robot's foot-contact force. The obtained force data is fed to the robot controller for ground-condition detection that helps the robot to move its legs. Finally, we succeeded in ground-surface self-detection with pressure sensors for robot movement on non-smooth surfaces.

Author's contributions

Conceived the plan: TKM, MMM; Authors: TKM, YO, DN, MMM, and HJM contributed equally in the work. Performed the expeirments: TKM, YO; Simulation and data analysis: TKM, MMM, and HJM; Wrote the paper: TKM, DN, MMM, and HJM. Authors have no competing financial interests.

References

1. Beebe, D. J.; Hsieh, A. S.; Denton, D. D.; Radwin, R. G.; *Sens. Actuators A, Phys.* , **1995**, *50*, 55. **DOI:** 10.1016/0924-4247(96)80085-9
2. Zhang, H.; So, E.; *IEEE Trans. Syst. Man Cybern.*, Part B, Cybern., **2002**, *32*, 57. **DOI:** 10.1109/3477.979960
3. Schmidt, P. A.; Mael, E.; Wurtz, R. P.; *Robo. Auton. Syst*., 2006, 54, 1005. **DOI:** 10.1016/j.robot.2006.05.013
4. Dargahi, J.; Parameswaran, M.; Payandeh, S.; *J. Microelectromech. Syst.*, **2000**, 9, 329. **DOI:** 10.1109/84.870059
5. Krishna, G. M.; Rajanna, K.; *IEEE Sens. J*., **2004**, *4*, 691. **DOI:** 10.1109/JSEN.2004.833505
6. Dahiya, R. S.; Valle, M.; Lorenzelli, L.; *IEEE Trans. Ultrason. Ferroelectr. Freq. Control*, **2009**, *56*, 387. **DOI:** 10.1109/TUFFC.2009.1048
7. Ohka, M,; Kobayashi, H.; Takata, J.; Mitsuya, Y.; 15th Int. Symp. Robo. Hum. Inter. Comm., pp. 214–219, **2006**. **DOI:** 10.1109/ROMAN.2006.314420
8. Yussof, H.; Takata, J.; Ohka, M.; Measurement principles of optical three-axis tactile sensor and its application to robotic fingers system, In Sensors: Focus on Tactile, Force and StressSensors, Rocha, J.G.; Lanceros-Mendez S.; I-Tech Publishers: Vienna, **2008**, pp. 123–142 **DOI:** 10.5772/6620
9. Nelson, T. J.; Van Dover, R. B.; Jin, S.; Hackwood, S., Beni, G.; *IEEE Trans. Magn. Mag*., **1986**, *22*, 394. **DOI:** 10.1109/TMAG.1986.1064386
10. Ando, S.; Shinoda, h.; Yonenaga, A.; Terao, J.; *IEEE Trans. Ultrason. Ferroelectr. Freq. Control*, **2001**, *48*, 1031. **DOI:** 10.1109/58.935720
11. Carlson, J. D.; Koester, S. P.; U.S. Patent 6283859 B1, **2001**.
12. Dahiya, R. S.; Metta, G.; Cannata, G.; Valle, M.; *IEEE Trans. Robot*., **2011**, *27*, 385. **DOI:** 10.1109/TRO.2011.2155830
13. Wiertlewski, M. ; Lozada, J. ; Hayward, V., *IEEE Trans. Robotics*, **2001**, *27*, 461. **DOI:** 10.1109/TRO.2011.2132830
14. Cutkosky, M. R.; Howe, R. D.; Provancher, W.; Force and tactile sensors, In Springer Handbook of Robotics, Siciliano, B.; O. Khatib, O. (Eds.); Springer-Verlag Berlin Heidelberg, **2008**. **DOI:** 10.1007/978-3-540-30301-5
15. Capisani, L. M.; Ferrara, A.; *IEEE Trans. Ind. Electron.*, **2012**, *59*, 3189. **DOI:** 10.1109/TIE.2011.2160510
16. Hogan, N; *IEEE /ASME Trans. Mechatronics*, **2014**, *19*, 1929. **DOI:** 10.1109/TMECH.2013.2294096
17. Bombled, Q; Verlinden, O.; *Multibody Syst. Dyn*., **2012**, *28*, 395. **DOI:** 10.1007/s11044-012-9305-z
18. Nagasaka, K.; Inaba, M.; Inoue, H.; Proc. of 17th Ann. Conf. Robo. Soci. of Japan, 1999, pp.1193-1194, (in Japanese).
19. Shimomura, M.; Shimizu, M.; Endo, K.; Furuta, T.; Okumura, Y.; Tawara, T.; Kitano, H.; JSME ROBOMEC, 2003, (in Japanese).
20. Suwanratchatamanee, K.; Matsumoto, M.; Hashimoto, S.; *IEEE Trans. Ind. Electron*., **2011**, 58, 3174. **DOI:** 10.1109/TIE.2009.2030217
21. KHR-3HV Humanoid Robot, Kondo Kagaku Co., Ltd. http://kondo-robot.com
22. Tekscan, Inc., USA, Force Sensors for Design. www.tekscan.com
23. Maiti, T. K.; Chen, L.; Miura-Mattausch, M., Koul, S. K.; Mattausch, H. J.; IEEE Electron Dev. Tech. Manuf. Conf., Japan, 259, **2017**. **DOI:** 10.1109/EDTM.2017.7947589
24. Maiti, T. K.; Miura-Mattausch, M., Koul, S. K.; Mattausch, H. J.; Proc. 8th Int. Conf. on Mech. Manuf., Japan, pp. 1-6, **2017**.
25. Caekenberghe, K. V.; *IEEE Micro. Mag*., **2012**, 13, 83. **DOI:** 10.1109/MMM.2011.2173984
26. Senturia, S. D.; Springer: USA, **2001**. **DOI:** 10.1007/b117574
27. Nathan, A.; Baltes, H.; Microsystem simulation, In Microtransducer CAD, Springer-Verlag Wien, **1999**, pp. 385 – 394. **DOI:** 10.1007/978-3-7091-6428-0
28. Mosser, V.; Suski, J.; Goss, J.; *Sens. Actuators A*, **1991**, *28*, 113. **DOI:** 10.1016/0924-4247(91)85020-O
29. Bechtold, T.; Schrag, G.; Feng, L. (Eds); Wiley-VCH Verlag GmbH & Co. KGaA, Germany, **2013**. **DOI:** 10.1002/9783527647132
30. Spong, M. W.; Hutchinson, S.; Vidyasagar, M.; John Wiley & Sons: USA, **2006**.
31. SparkFun Electronics, USA, Force Sensitive Resistor Hookup Guide. https://learn.sparkfun.com/tutorials/force-sensitive-resistor-hookup-guide

